

EUROPA LANDER TRAJECTORY DESIGN USING LISSAJOUS STAGING ORBITS

Ricardo L. Restrepo,^{*} Ryan P. Russell,[†] Martin W. Lo[‡] and Timothy P. McElarth[§]

Lissajous orbits and approximation of their invariant manifolds are used to generate landing trajectories to the surface of Europa. Each lissajous is discretized into individual revolutions that each resemble a periodic orbit. The unstable manifolds of each individual revolution propagated forward in time generate more surface coverage than manifolds of simple libration point orbits such as halo or Lyapunov orbits. The stable manifolds propagated backwards in time from the individual lissajous revolutions provide direct connections to the last phase of a moon tour. The strategy developed produces ballistic landing trajectories with a wide surface coverage, and allows for the decoupling of the landing and moon tour phase by using the lissajous as an intermediate staging orbit. The multiple revolutions of the lissajous, multiple departure times along each revolution, multiple quasi periodic options at each energy, and multiple energies of the lissajous family provide many degrees of freedom in the design process.

INTRODUCTION

Europa, an icy moon of Jupiter, is currently one of the most attractive places for scientific exploration due to its potential to harbour life.^{1,2} In order to deeply explore this moon, a probe that lands on the surface might be preferable to an orbiter or flyby-type mission, as in situ measurements provide direct access to search for biosignatures. Low-energy trajectories provide a fuel-efficient mechanism to approach a moon of a planetary satellite system (a typical two-body patched conic design would be too expensive for this type of mission).^{3,4} To achieve capture at Europa, a general established strategy for orbiter missions is to use a moon tour after Jupiter insertion to gradually reduce the two-body energy of the spacecraft.^{5,6,7,8,9} The moon tour involves using three-body gravity assists of Ganymede, Europa, and possibly Callisto (depending on the science and engineering priorities) in a resonant hopping sequence.^{10,11,12} Once close enough to Europa, the natural access to a capture orbit is via the L_2 gateway.^{13,14,15} Libration point orbits and their manifolds provide the capture mechanisms and are also useful as staging orbits for phasing purposes.¹⁴ To land on the surface of the icy moon, an additional phase is required that connects the capture phase to a target landing location.

^{*}Graduate Student, Department of Aerospace Engineering and Engineering Mechanics, The University of Texas at Austin, W.R. Woolrich Laboratories, C0600. 210 East 24th Street, Austin TX 78712-1221; ricardo.rpo@utexas.edu.

[†]Associate Professor, Department of Aerospace Engineering and Engineering Mechanics, The University of Texas at Austin, W.R. Woolrich Laboratories, C0600. 210 East 24th Street, Austin TX 78712-1221; ryan.russell@utexas.edu

[‡]Jet Propulsion Laboratory, California Institute of Technology, Pasadena, CA 91109,USA; martin.w.lo@jpl.nasa.gov

[§]Jet Propulsion Laboratory, California Institute of Technology, Pasadena, CA 91109,USA; timothy.p.mcelarth@jpl.nasa.gov

Several studies have explored capture mechanisms to low science orbits around Europa (see for example References 5, 16, 17, 18, 19, 20). Nevertheless, literature on landing strategies is more scarce (to the best knowledge of the author) together with a lack of comprehensive information on how to target specific landing sites addressing standard missions constrains.^{9, 21} A lander-type mission can have numerous mission constraints, including lighting conditions at the time of landing, staging locations to decouple the approach to Europa, a broad range of desired landing latitudes for surface coverage, etc. These constraints lead to a highly complicated trajectory design. For this reason it is preferable to divide the trajectory design after Jupiter insertion into three separate steps, breaking the highly coupled problem into independent phases: 1) the moon tour, 2) the capture at Europa, and 3) phasing the landing. In this paper, the last two phases of the problem are considered. The strategy of building the missions by phases decouples the highly nonlinear problem and allows each phase to be studied individually, reducing the complexity of the problem.

Lissajous orbits and their invariant manifolds are the dynamical structures used to frame the capture, phasing, and landing of the Europa lander problem. Their approximate unstable invariant manifolds, propagated forward in time, are used as potential landing trajectories, while the stable invariant manifolds, propagated backward in time, are used to connect with the last resonant of the hopping sequence. Lissajous orbits are three-dimensional quasi-periodic structures that form a two-dimensional torus around the libration points of the circular restricted three-body problem (e.g., L_2 in our case).²² The invariant manifold of a torus is a solid object. The set of trajectories that conform this solid structure provide more coverage over the surface of Europa than the surface formed by the invariant manifolds of simple periodic orbits (e.g., halo or Lyapunov orbits). Additionally, there are only two halo orbits around L_2 (northern and southern) and one Lyapunov orbit at a given energy level or Jacobi constant. In contrast, there exists a continuous family of lissajous orbits at a fixed energy level. Hence lissajous orbits are chosen as the main dynamical structure to solve the lander problem.

The computation of manifolds of invariant tori is known to be a challenging problem in dynamical system theory, and different sophisticated procedures have been proposed to address it.^{23, 24, 25, 26, 27} In the current work, a simplified approach is implemented. The surface of the torus is filled by computing individual lissajous revolutions (revs) with a small phase difference between them. Each lissajous rev is used as an approximate periodic orbit (PO) and the invariant manifolds of each approximate PO are computed. The sum of the manifolds of each of the lissajous revs approximates the manifold of the entire torus. This simplification is possible due to the nature of the problem addressed here, where only individual lissajous revs, or fractions of revs, are used for staging. The computation of the individual lissajous revs is done using a similar approach to that in Howell and Pernika,²⁸ where the analytical expansion developed by Richardson and Cary²⁹ is used as the initial conditions for a multiple shooting technique. Although more robust techniques have been developed to generate quasi-periodic orbits around libration points (as those in Ref. 30, 22), the adopted numerical approach produces satisfactory results for the generation of individual lissajous revs.

This paper is organized as follows. First, a detailed description of a Europa lander problem is presented, along with the assumed mission constraints. A first attempt to solve the problem via the patched periodic orbit (PPO) model is described. In search of a methodology that provides a wider range of solutions, lissajous orbits and their invariant manifolds are introduced as a replacement for the building blocks of the PPO model. In the following section a technical description of the generation of lissajous orbits and their approximate invariant manifolds is presented. A pre-generated

database of individual lissajous revs is then used to compute their approximate unstable invariant manifold trajectories and filter those that reach the surface of Europa by satisfying all the mission constraints. In the section that follows, a resulting database of landing trajectories is presented in a longitude/latitude map, showing the range of possible landing locations reachable with trajectories emerging from lissajous orbits. Finally, end-to-end trajectory examples are shown, where each lissajous rev, from where landing trajectories depart, is connected to resonant orbits by the backward propagation of its stable manifold trajectories.

Mission Constraints

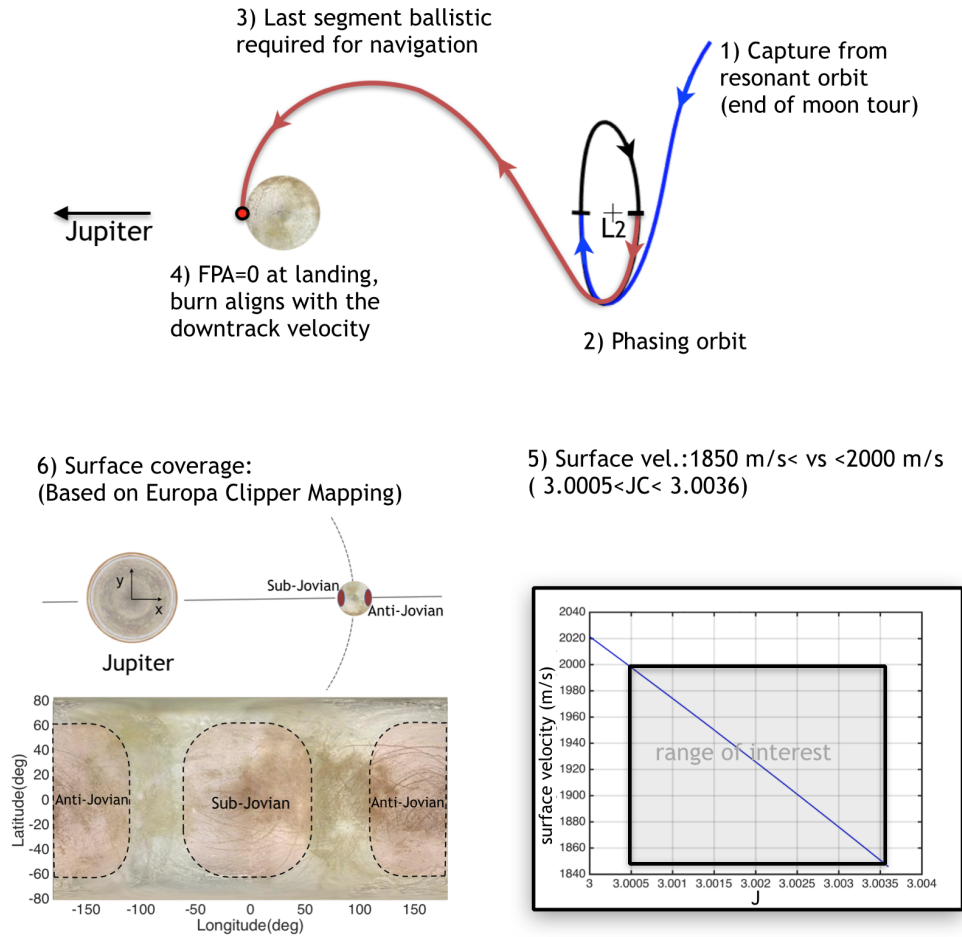


Figure 1. Europa probe lander problem description and mission constraints

The goal of the problem at hand is to develop a general trajectory design strategy to land on the surface of Europa, keeping in mind a few important constraints, shown in Figure 1. (1) The spacecraft is assumed to approach Europa from a resonant hopping sequence. The capture at Europa then occurs from the last resonant orbit of the sequence. (2) A staging orbit is used as a temporary station to decouple the approach to Europa with the location and timing of landing. This orbit allows specific mission requirements, such as having good lighting conditions or direct communication with Earth at the time of landing, to be incorporated into the design strategy. (3) The last segment before landing must be ballistic, due to the fact that there is, in general, no time to perform deterministic

maneuvers and correct any errors due to these maneuvers before performing an accurate landing. (4) Assuming a solid rocket motor (SRM) during the de-orbit, descent, and landing (DDL) stage, the landing must occur at a flight path angle of zero, i.e., at periapse, due to the fact that the position uncertainty for an SRM aligns with the downtrack velocity, therefore minimizing any errors in the downtrack direction at landing. (5) The surface velocity of the spacecraft at Europa is constrained to range between 1840 to 2020 m/s. The lower limit comes from the minimum energy at which the L_2 gateway opens ($J = J_{L_2}$), allowing for ballistic captures. Note that the surface velocity is directly related to the energy or Jacobi constant, as shown in the plot of velocity vs. J in Figure 1. At lower velocities, a deterministic maneuver would be necessary to arrive at the phasing orbit from a resonant orbit. The upper limit on the surface velocity constraint is chosen by the upper limit of the low energy regime ($J = 3$), which is the maximum energy at which ballistic captures around Europa are possible. (6) The last and final constraint is the desire for global surface coverage at landing. Currently, not enough is known about this moon to pick a specific landing location. However, a mission set to study Europa through a series of flybys in the mid-2020s will provide a map that can be used in the future for the selection of a scientifically rich landing site. This mission, called Europa Clipper, will only map a region around the sub-Jovian and anti-Jovian sides of Europa due to flyby geometry constraints.^{31,32} Because of this, a general strategy that produces trajectories that can globally cover these regions of interest is desired.

Example Solution Obtained Via the PPO Model

The patched periodic orbits model, described in Ref.,³³ provides some point solutions that satisfy most of the constraints of the Europa lander trajectory problem previously described. The PPO model allows to build complex low-energy trajectories simplifying the design process by using a compatible sequence of planar x -axisymmetric periodic orbits and patching them together at their perpendicular x -crossing. The discontinuities between the sequence of selected periodic orbits are generally small and can be considered acceptable at an early design stage. A differential corrector or an optimizer can be used at a more advanced stage in order to generate a continuous trajectory. The PPO model provides trajectories that naturally incorporate staging orbits, since each segment of the sequence is a periodic orbit itself. The method also provides direct connections between resonant orbits and libration point orbits (i.e., Lyapunov orbits around L_1 and L_2) through a special set of POs that approximate heteroclinic connections between the aforementioned pair of orbits, known as *connecting resonances*.

Figure 2 shows two point solutions of the Europa lander problem, constructed by using the patched periodic orbits model.³³ In these examples, a spacecraft, initially in a 5:6* resonant orbit with Europa, is transferred to a Lyapunov orbit around L_2 throughout a connecting resonant orbit of the family $H_{5:6-LL_2}$ [†]. Once around L_2 , this weakly captured orbit can be used as a temporary station to stage the next phase of the mission. Then, as shown in Figure 2(a), half a period of the periodic orbit Hm_2 is used to bring the spacecraft from the Lyapunov orbit to the surface of Europa exactly at the sub-jovian point (i.e., 0° latitude and 0° longitude). In the example shown in Figure 2(b), the spacecraft is instead transferred from the Lyapunov at L_2 to a Lyapunov at L_1 by using another connecting PO known as Hg . Then, half a period of the periodic orbit Hm_1 is used to bring the spacecraft to the surface of Europa exactly at the anti-jovian point (i.e., 0° latitude and

*In a $p:q$ resonance, p is the number of revs of the spacecraft around Jupiter in an inertial frame for q revs of Europa.

† The $H_{5:6-LL_2}$ family is a special set of periodic orbits that approximate heteroclinic transfers between simple 5:6 resonance and L_2 Lyapunov orbits. For more details see Ref. 34

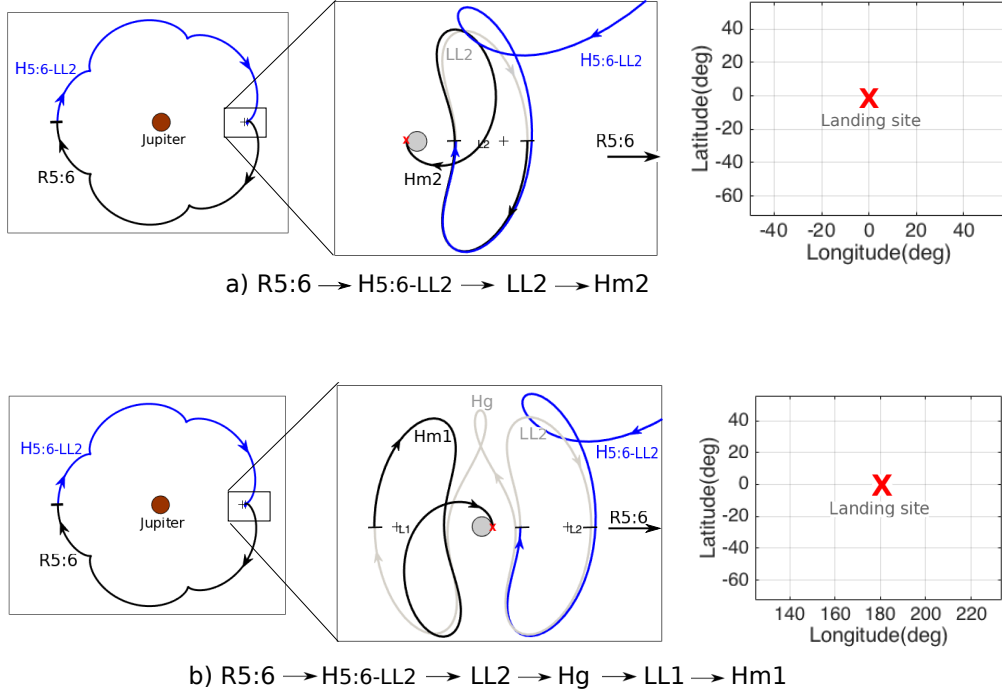


Figure 2. Example solutions for a Europa lander mission via PPO model.

180° longitude). The POs Hm_1 and Hm_2 , used in the last segment of the landing trajectories in Figure 2, are chosen at $J = 3.0018$. This is the Jacobi constant value at which these two families end, crashing at the surface of Europa, i.e., providing two landing solutions with $\gamma = 0$. At this Jacobi constant, the surface velocity of the spacecraft is 1930 m/s.

The two example solutions shown in Figure 2 generated with the PPO model satisfy most of the constraints of the Europa lander problem. However, constraint number 6 (full landing sites coverage) cannot be fully satisfied, since the PPO model is constrained to the plane, and therefore, only landing sites at the equator of Europa can be achieved. In order to obtain higher latitude landing solutions, a new method is implemented, which still keeps the general strategy of solving the problem by individual phases as in the PPO model, but provides a wider space of solutions.

EUROPA LANDER TRAJECTORIES VIA LISSAJOUS ORBITS

Lissajous orbits are quasi-periodic structures associated to each of the collinear libration points of the circular restricted three-body problem (i.e., L_1 , L_2 and L_3). These three-dimensional structures are bounded trajectories constrained to the surface of a two-dimensional object, known as an invariant torus. Computing the manifolds of an invariant torus can be complicated and computationally expensive. To simplify the process, individual revolutions (revs) of lissajous trajectories are considered as approximate periodic orbits. For each lissajous rev, approximate stable and unstable manifolds are computed by using standard techniques to compute the invariant manifolds of periodic orbits.^{18,35,15} The trajectories that depart from the lissajous revs, conforming the approximate unstable manifolds, are propagated forward in time, and those that arrive with zero flight path angle ($\gamma = 0$) at the surface of Europa (i.e., periaapse) are considered potential landing legs. In general,

any trajectory that crashes on the surface of Europa could be a potential landing trajectory; however only trajectories that arrive at periapse, i.e., parallel to the surface, are considered in order to minimize errors that align with the downtrack velocity (constraint *No* 4). The approximate stable invariant manifolds, propagated backward in time, are used to connect with the last resonance of the moon tour (constraint *No* 1). Each lissajous is used as a temporary station or staging orbit to satisfy the phasing requirement (constraint *No* 2). The generation of lissajous orbits and their approximate invariant manifolds are described in the following sections.

Lissajous Orbit Generation

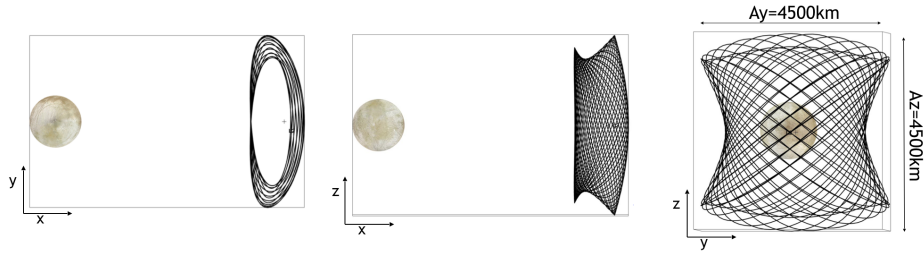
There are two fundamental types of periodic motion around the collinear libration points associated to two families of periodic orbits: the *planar* and the *vertical* Lyapunov orbits. Planar Lyapunov orbits are constrained to the plane of motion of the primaries (x-y plane), and vertical Lyapunov orbits are dominated by an out-of-plane component crossing the x-y plane only at the collinear point.²² Each of these fundamental families have an associated frequency that is a function of the amplitude of the orbit. At certain energy levels, a third type of periodic orbit emerges, known as a Halo orbit. The out-of-plane and the in-plane frequencies for these three-dimensional orbits are equal.³⁶ Quasi-periodic structures exist around the vertical Lyapunov and the Halo orbits, known as lissajous²⁸ and quasi-halo orbits,³⁷ respectively. These quasi-periodic structures reside on the surface of an invariant torus around the corresponding periodic orbit. In this work, individual revs of lissajous orbits are used as the fundamental elements for the trajectory design.

Lissajous orbits are symmetric with respect to the x-y plane and the x-z plane, and can be characterized by an in-plane amplitude A_y and an out-of-plane amplitude A_z . Lissajous orbits can be periodic for exact resonances between the in-plane and our-of-plane frequencies, but in general they are not, and in this case their trajectories can exist at any point in the surface of a two-dimensional torus. Two initial phases ϕ and ψ can be used to define a particular trajectory over the torus, where ψ is a phase associated to the out-of-plane motion and ϕ to the in-plane phase²⁸ (see Figure 3) .

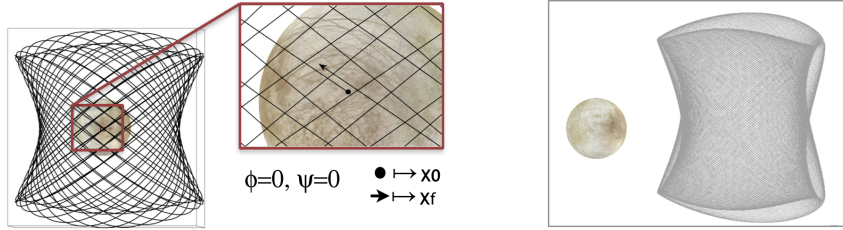
Figure 3(a) shows three different views of a lissajous orbit centered around L_2 in the Jupiter-Europa system, with associated amplitudes $A_y=4500$ km and $A_z=4500$ km. The initial conditions of the trajectory are such that it begins in the x-y plane, i.e., $\psi = 0^\circ$ and $y = 0$, that is, with a phase $\phi = 0^\circ$. Figure 3(b) shows the trajectory propagated for 27 revs, where the in-plane phase completes approximately 360° , but not exactly.

The non-periodicity of the orbit is observed in this example. In Figure 3(c), the trajectory is propagated for 2000 revs, highlighting the two-dimensional structure of the torus.

A variety of methods on the generation of quasi-periodic orbits around libration points have been developed. From the analytic approximations, Farquhar and Kamel³⁸ used the method of Linstedt-Poincaré to produce third order expansions. Richardson and Cary developed a third-order approximation of quasi-periodic motion via the method of multiple time scales.²⁹ Jorba and Masdemont investigated the dynamics around the libration points using center manifold reduction,³⁹ and higher order formulas are presented by Gómez.³⁷ Based on these analytical approaches, Howell and Pernika presented a numerical shooting approach for correcting analytic third and four order expansions.²⁸ Barden and Howell applied multiple shooting methods to find quasi-periodic structures with application to formation flyin⁴⁰g. Gómez and Mondelo developed a scheme for computing two-dimensional quasi-periodic tori using Fourier analysis,⁴¹ and Kolenen et al.²² presented a fully-numerical and fast method for finding quasi-periodic orbits around libration points based on



a) Lissajous parameters



b) 27 Revs propagation (liss. does not close) c) 2000 Revs propagation covering a Torus

Figure 3. Lissajous orbit example around L_2 in the Jupiter-Europa system

multiple Poincaré maps.

As the strategy proposed in this work requires only the computation of individual lissajous revs, the robustness and generality of the latest developments is replaced by simplicity in the implementation. Hence, the multi-shooting technique of Howell and Pernika combined with the Richardson and Cary expansions is adopted. This numerical approach produces satisfactory results for the generation of individual lissajous revs. The inputs for the analytic fourth-order expansion algorithm are the amplitudes A_y and A_z , the initial phases Ψ and Φ , and the number of revolutions. The outputs of the analytic procedure are a set of state vectors along the approximate trajectory. The integrated path between state points are not necessarily continuous, and a multiple-shooting technique is employed to generate a continuous trajectory in a two level iterative process.²⁸ Lissajous trajectories are highly unstable, and converged solutions with multiple revolutions cannot be reproduced by simply propagating the initial state. Small correction maneuvers along the path are required. The 27 revs lissajous trajectory shown in Figures 3(a)-(b) and Figure 4(a), incorporate several trajectory correction maneuvers.

The general structure of a lissajous torus can be obtained by generating individual lissajous revs all around its surface. This depiction is shown in Figure 4. In Figure 4(a) one single rev is highlighted in red. The initial conditions of this lissajous rev start at the x-y plane ($\psi = 0$) with $\phi = 0$, and it is propagated for one pseudo-period (T_{rev}) i.e., until it completes a full out-of-plane cycle, returning to the x-y plane. Note that the pseudo-period T_{rev} , is equivalent to the period related with the out-of-plane frequency. To approximate the global structure of a lissajous torus, individual revs are generated with a small in-plane phase difference ($\Delta\phi$) in their initial conditions. In the example shown in Figure 4(b), 200 lissajous revs are used to approximate a lissajous torus with amplitudes $A_y=4500$ km and $A_z=4500$ km, with a phase shift of $\Delta\phi = 1.8^\circ$ between revs. For simplicity ψ is always set to zero. This example represents the general strategy used to compute all the lissajous

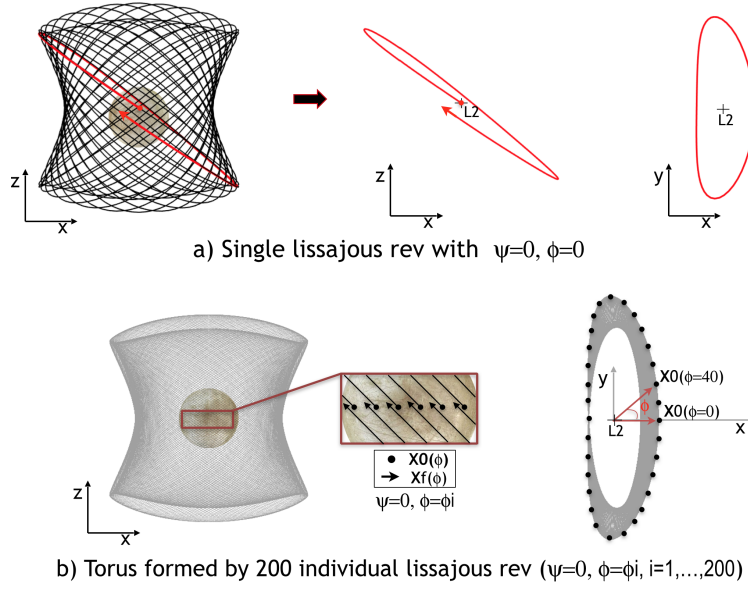


Figure 4. Lissajous orbits discretized by individual revs

trajectories generated in this work.

Generation of Invariant Manifolds of lissajous Orbits

Each lissajous rev, computed as described in the previous section, acts as a good approximation of a periodic orbit, which allows for the computation of approximate invariant manifolds. The invariant manifold of an entire lissajous torus can therefore be approximated by combining the approximate invariant manifolds of each of the individual revs that approximate the torus. In the following section, a brief description on how to compute the invariant manifolds of a periodic orbit is presented, followed by how this procedure is adapted to compute the approximate invariant manifolds of individual lissajous revs

Invariant manifolds of periodic orbits The computation of the stable and unstable invariant manifolds of a periodic orbit are obtained by perturbing each point of the orbit along a specific stable and an unstable direction. This procedure is described in detail in Ref. 18, 35. The direction of the perturbation is given by the eigenvectors of the monodromy matrix ($\Phi(T, t_0)$), which is the state transition matrix (STM) evaluated after one orbit period (T). Recall that the STM $\Phi(t_i, t_0)$ is the solution of the variational equations of the CRTBP evaluated at time t_i . The eigenvalues of the monodromy matrix of an unstable periodic orbit will in general contain four eigenvalues of unit magnitude and two that form a complementary pair of asymptotically stable ($\lambda < 1$) and unstable ($\lambda > 1$) values. The corresponding eigenvectors associated to the unit magnitude eigenvalues are a complex conjugate pair and a repeated real pair. The additional two eigenvalues are associated to two fully real vectors, which are the ones used to excite the stable and unstable motion around the periodic orbit. The eigenvector $\mathbf{V}_u(t_0)$ with real eigenvalue greater than 1 provides the unstable direction; the eigenvector $\mathbf{V}_s(t_0)$ with reciprocal eigenvalue less than 1 provides the stable direction. To compute the stable and unstable directions at any point over the orbit, the STM is used as a linear mapping. For example, the unstable directions along the orbit are given by:

$$\mathbf{V}_u(\tau) = \mathbf{\Phi}(\tau, t_0)\mathbf{V}_u(t_0) \quad (1)$$

where τ is a normalized variable ($\tau = 0 \rightarrow 1$) introduced to represent the time discretization along one period of the orbit, such that $t_i = t_0 + \tau T$. The manifold trajectories are obtained by propagating the perturbed states

$$\mathbf{X}_u(\tau) = \mathbf{X}(\tau) \pm \epsilon \hat{\mathbf{V}}_u(\tau) \quad (2)$$

where $\hat{\mathbf{V}}_u(\tau) = \mathbf{V}_u(\tau)/\|\hat{\mathbf{V}}_u(\tau)\|$, and ϵ is a small parameter ($\epsilon \ll 1$) that represents the magnitude of the perturbation.

Approximate invariant manifolds of lissajous orbits The intricate process of computing the invariant manifolds of an entire lissajous torus is simplified by combining the approximate invariant manifolds of the individual lissajous revs that conform the full torus. The STM is propagated for each rev from t_0 to T_{rev} to obtain an *approximate* monodromy matrix $\mathbf{\Phi}(T_{rev}, t_0)$. The stable and unstable invariant manifolds for each lissajous rev are computed using the same procedure as that for periodic orbits. Note that due to the symplectic nature of the STM, the eigenvalues of this approximate monodromy matrix still come in reciprocal pairs. However, the two unity magnitude real eigenvalues found in a periodic solution no longer exist; they are now near unity, corresponding to a marginally stable and unstable eigenvector direction. The two remaining real eigenvectors, corresponding to highly stable and unstable directions, are the ones used to generate the approximate invariant manifolds of each lissajous rev, and Eq. 2 is used to compute the perturbed states. The value of $\epsilon = 10^{-6}$, commonly used in literature,^{35,15} is used for this implementation. Note that by fixing the value of ϵ , a degree of freedom is lost. However, variations in ϵ , corresponding to different departure times, are equivalent to solutions associated with different values of τ (see Reference 14).

Figure 5 shows a schematic of an unstable manifold trajectory propagated forward in time at τ_i (blue) and a stable manifold trajectory propagated backwards in time at τ_j (red) for one lissajous rev. Each lissajous rev is discretized in 100 points from $t_0 \rightarrow T_{rev}$ to generate 100 stable, and 100 unstable manifold trajectories per rev. Note from Eq. (2) that there are directions to perturb (positive and negative) for each stable and unstable eigenvector. For example, by perturbing in the positive direction of the unstable eigenvector, trajectories that go towards Europa are obtained, while a perturbation in its negative direction will produce trajectories that escape from Europa. The sign of the perturbation is selected such that unstable manifolds move towards Europa, and the stable manifolds move away from Europa.

Figure 6 shows the unstable manifold of one a lissajous rev propagated forward in time. The propagation is stopped when first periapse is reached. The projection of each periapse over the surface of Europa is shown in a latitude/longitude map, which are observed as an ellipse-like object. Two types of solutions are obtained, those that arrive at Europa below its surface (sub-surface solutions shown in grey) and those that arrive above the surface (shown in red). If the manifold of the lissajous rev were actually computed as a continuous set of trajectories, two solutions would arrive at Europa exactly at the surface*. However, due to the discretization of the manifold generation (100 pts per rev), exact landing solutions are not guaranteed, and those that arrive between 0 to 40 km of altitude are selected as potential landing trajectories. The two landing trajectories are shown

*This assumption is valid with exception of the cases in which a gap in the approximate manifold, caused by the non-periodicity of the lissajous rev, coincide with the surface of Europa. See gap in the landing trajectory map in Figure 6.

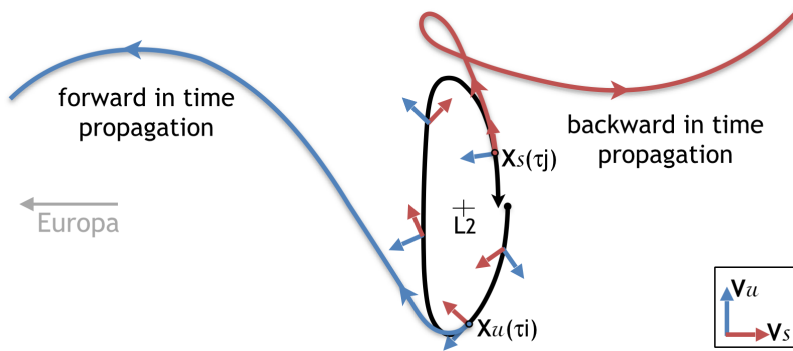


Figure 5. Schematic of stable (red) and unstable (blue) manifolds for one lissajous rev.

in magenta in the trajectory plot, and their corresponding landing location are represented in the latitude/longitude map as (two) black dots.

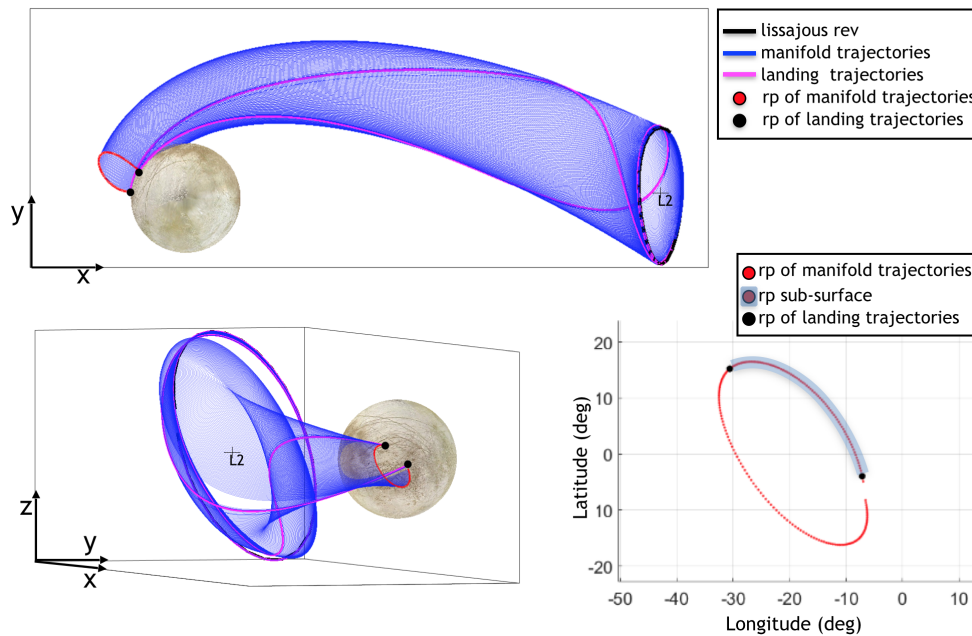


Figure 6. One lissajous rev, its unstable invariant manifold, and potential landing trajectories shown in a latitude/longitude map.

Figure 7(a) shows the stable manifold of one lissajous rev propagated backward in time. These trajectories are the ones used to connect with the last part of the tour phase. The general strategy to approach Europa is through a sequence of high altitude three-body flybys to reduce the spacecraft's two-body energy with respect to Jupiter. For this sequence of flybys to be possible they have to occur through a set of resonant sequences in order to guarantee the periodicity of the encounter of the spacecraft with Europa. Therefore, the leg of the trajectory that connects with the lissajous orbit (forward in time) must be a resonant trajectory. This leg is selected from the set of trajectories that compose the stable manifolds that arrive at the lissajous rev, and they are computed backwards in time. In order to determine the value of the resonance associated to each manifold trajectory, each trajectory is propagated backwards in time until it crosses the negative x-axis (left side of Jupiter

in the rotating frame), where the negative x -crossing acts as a Poincare section. Using the state of each trajectory at this intersection, the osculating semi-major axis with respect to Jupiter is used to directly relate the trajectory segment with a resonance value. Figure 7(b) shows the osculating semi-major axis for each manifold trajectory that departs from the lissajous rev as a function of τ . Due to the sinusoidal behavior of this function, there are always two locations on a lissajous rev (characterized by τ) from where manifold trajectories leave reaching the same resonance. The range of resonances reachable from the lissajous rev shown in Figure 7(b) varies from 5:6 to 7:8. In the example, two manifold trajectories associated with a 6:7 resonance are shown in magenta. Their corresponding τ values are $\tau = 0.31$ and $\tau = 0.93$.

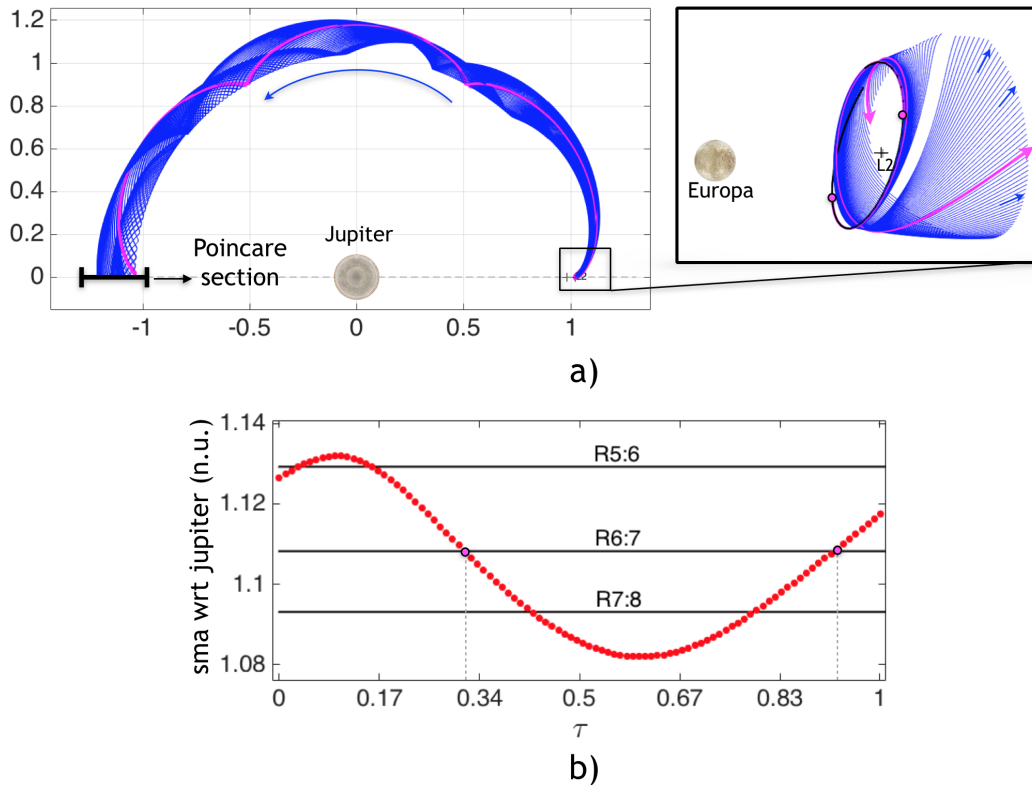


Figure 7. a) Backward propagation of the stable manifold of a lissajous rev. b) Semi-major axis map (sma) of the manifold trajectories as a function of τ showing accessible resonance connections.

MAPPING MANIFOLD TRAJECTORIES TO LANDING SITES

Using the technique described in the previous section to generate lissajous orbits and their approximate invariant manifolds, an entire database of lissajous orbits and potential landing trajectories is generated. The database of lissajous orbits is generated by sweeping A_y from $1000 \text{ km} \leq A_y \leq 12000 \text{ km}$ in 500 km intervals and A_z from $2000 \text{ km} \leq A_z \leq 12000 \text{ km}$ by intervals of 100 km, for a total of 1100 lissajous. Each lissajous orbit is constructed by 200 individual revs (each one approximating a periodic orbit) for a total database of 220,000 lissajous revs. In order to search for potential landing trajectories, the unstable invariant manifolds of each individual rev is generated by discretizing each rev in 100 points and perturbing along the unstable direction of each point.

The approximate unstable manifold of each full lissajous orbits is, therefore, comprised by 20,000 trajectories. The entire database of lissajous orbits produces 22M manifold trajectories, which then need to be searched over for potential landing trajectories.

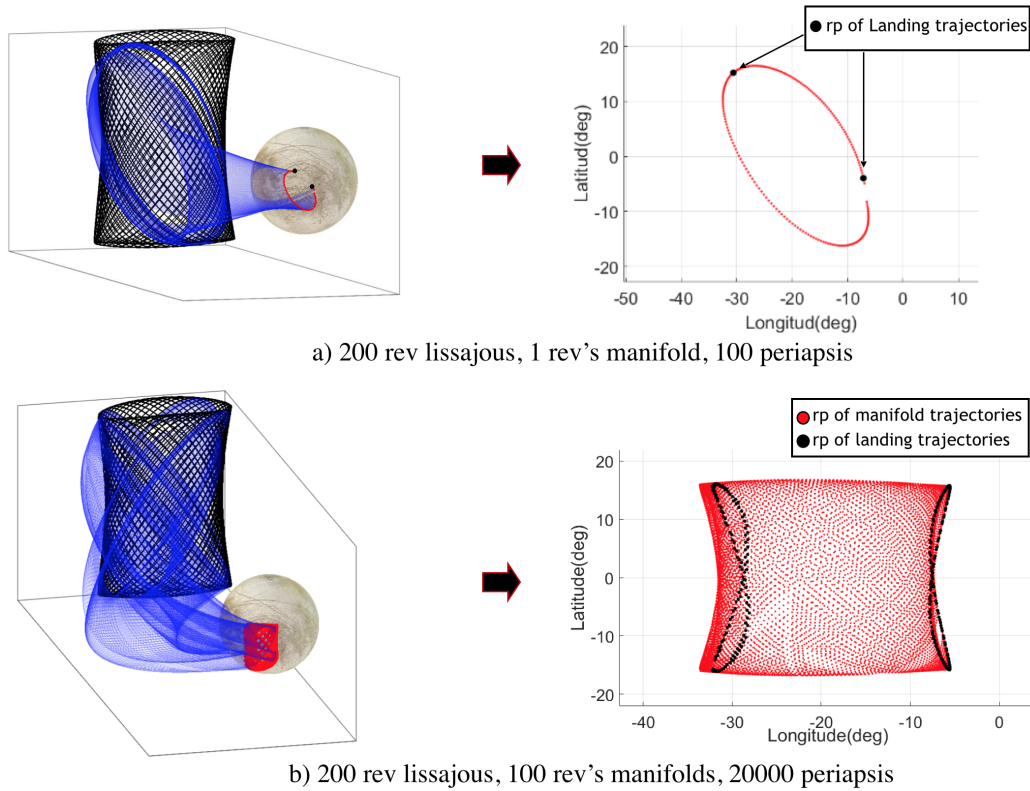


Figure 8. The approximated unstable invariant manifold of a full lissajous orbit ($A_y = 2000$ km, $A_z = 3000$ km) and potential landing trajectories

Figure 8 shows a lissajous orbit with parameters $A_y = 2000$ km and $A_z = 3000$ km, composed by 200 individual lissajous revs. Figure 8(a) shows the 100 trajectories that compose the unstable invariant manifolds of one of the lissajous revs. The periapses of two potential landing trajectories are depicted as black points in both the trajectory plot (left) and in the latitude/longitude map (right). Figure 8(b) shows the invariant unstable manifolds of each of the 200 revs that compose the full lissajous orbit. The latitude/longitude map shows the projection of the corresponding periapsis (20,000 in total). In this figure it is evident that the manifold of an entire lissajous (or a torus) is a solid object, in contrast with the manifold of a single rev (Figure 8(a)) or a simple periodic orbit, which is a tube. As a consequence, instead of having two landing opportunities, a full set (continuous in a non discretized model) of potential landing trajectories is obtained. The periapsis of these potential landing trajectories are observed as two figure “8” in the latitude/longitude map of Figure 8(b) (right). Therefore, by using lissajous orbits instead of simple periodic orbits (i.e., halos or Lyapunov orbits) the surface coverage for landing opportunities is greatly increased, going from two sites per orbit to continuous lines with a wide range of latitudes.

In the results shown in Figure 8, the manifold trajectories are propagated until first periapsis is reached. A wider range of surface coverage is obtained by continuing the propagation of the

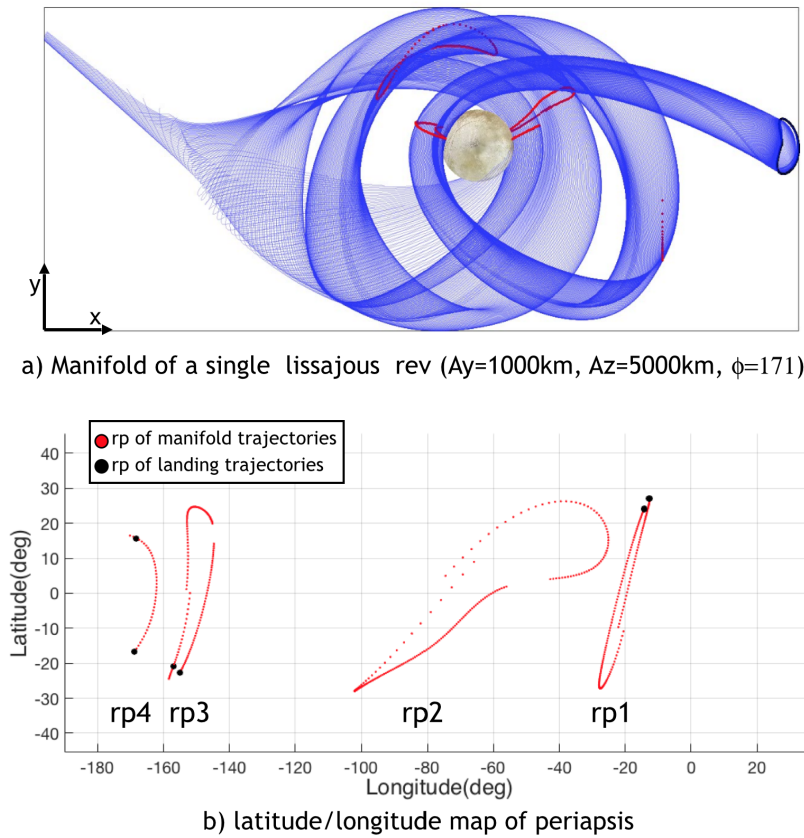
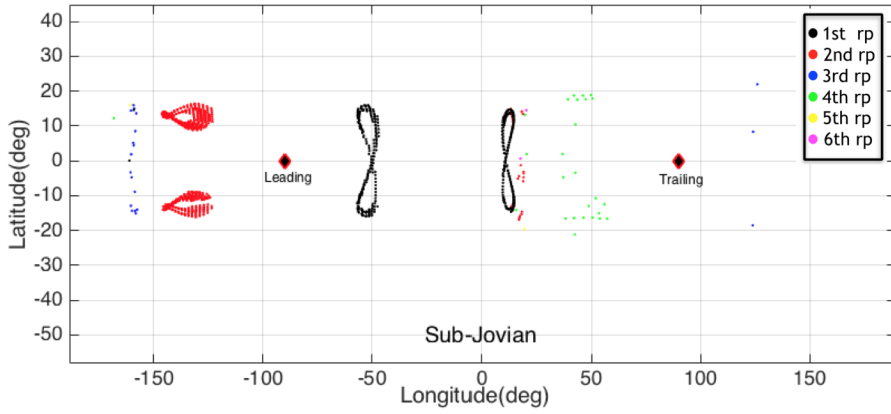


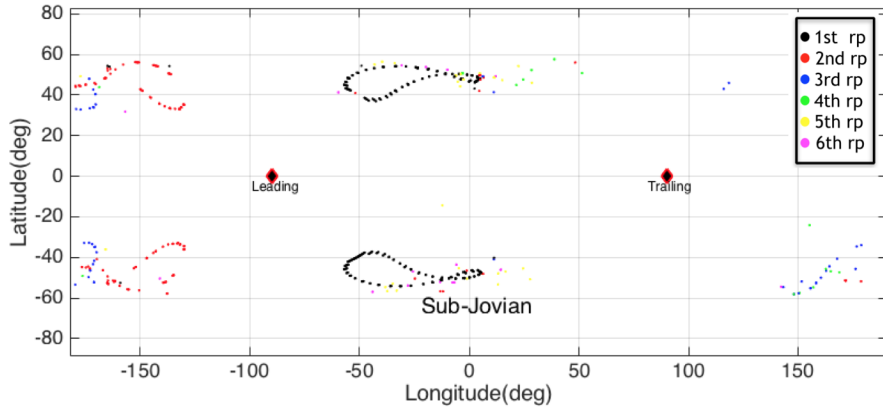
Figure 9. Manifold trajectories of a single lissajous rev with multiple periapsis passes

trajectories that do not crash over the Europa surface, allowing multiple periapsis before landing condition is achieved. Hence, the search for landing trajectories is implemented by propagating each trajectory of the unstable invariant manifolds forward in time until: 1) the trajectory crashes, 2) the trajectory escapes the sphere of influence of Europa, or 3) a maximum integration time is reached. The sphere of influence of Europa is roughly estimated as a sphere with radius equal to the distance between Europa and L_1 ; the maximum integration time is set to 10 days. Figure 9(a) shows the propagation of the manifold trajectories of one lissajous rev under the aforementioned stopping conditions. The manifold propagation includes four periapsis passes. Figure 9(b) shows the projection of the periapsis on a latitude/longitude map as red dots, and those associated with landing trajectories are depicted as black dots. In total, six landing trajectories are detected, two each at first, third and fourth periapsis. The second periapsis of the manifold occurs far from Europa with no potential landing trajectories.

Figure 10(a) shows a periapsis map of landing trajectories obtained from the manifolds of a full lissajous orbit with parameters $A_y = 2000$ km and $A_z = 3000$ km. The landing solutions are colored by their periapsis number. Two figure “8” of landing coverage in the sub-Jovian side of Europa are obtained from the first periapsis pass (black), similar to the result shown in Figure 8. The second periapsis produces two additional curves (red) in the anti-Jovian side of Europa, around 130 degrees of longitude west. The thickness of these curves is due to the tolerance imposed on the periapsis



a) Landing sites coverage from Lissajous $A_y=2000\text{km}$, $A_z=3000\text{km}$



b) Landing sites coverage from Lissajous $A_y=4000\text{km}$, $A_z=10000\text{km}$

Figure 10. Landing site coverage from manifold trajectories of full lissajous orbits (200 revs), allowing multiple periapsis passes

altitude to filter the landing trajectories (i.e., between 0 to 40 km). Solutions from the third (blue) and fourth (green) periapsis appear in the anti-Jovian and the sub-Jovian sides, respectively, and are observed as scattered points. The dispersion of these solutions is due to two reasons: first, most of the trajectories for this particular example crash on the Europa surface within the first two periapsis passes; and second, as the manifold evolves over time, it gets wider, with more space between trajectories, due to the discretization of the model, and hence, reaching less landing trajectories. Notice that all the landing solutions shown in Figure 10(a) are limited to latitudes $< |25|$ degrees. In contrast, landing solutions obtained from a lissajous orbit with parameters $A_y = 4000$ km and $A_z = 10000$ km, shown in Figure 10(b), produce solutions that cover latitudes between 30 to 60 (and -30 to -60) degrees. Thus, the latitude coverage is dependent on the lissajous orbit size.

Latitude/Longitude Coverage Maps

After filtering the 22M manifold trajectories, computed from the database of lissajous orbits, approximately 400k landing trajectories are obtained. The entire set of landing solutions is shown in Figure 11, colored by periapsis number. First periapsis solutions fill up mostly the sub-Jovian

region, while the anti-Jovian side is predominantly reached by second and third periapsis passes. Additional periapsis reach both the sub-Jovian and the anti-Jovian faces of Europa. Two gaps around the leading and the trailing side of the moon are observed, where the lack of landing solutions appears to be a consequence of the natural flow of the lissajous manifolds, that is to say, the natural flow of the dynamics of the system. Luckily, these unreachable regions coincide with zones of less interest for the the Europa lander problem at hand (see constraint *No 6* in Figure 1), which is related to the non-observable zones for the Europa Clipper mission. A natural concentration of solutions is observed in regions of low latitudes (e.g., < 30 degrees), since high latitudes are only reachable by manifolds coming from high Az amplitude lissajous orbits. Regions with sparse point solutions can be improved by repeating the trajectory generation with a more refined search (i.e., more revs per lissajous orbits, and more manifold trajectories per rev).

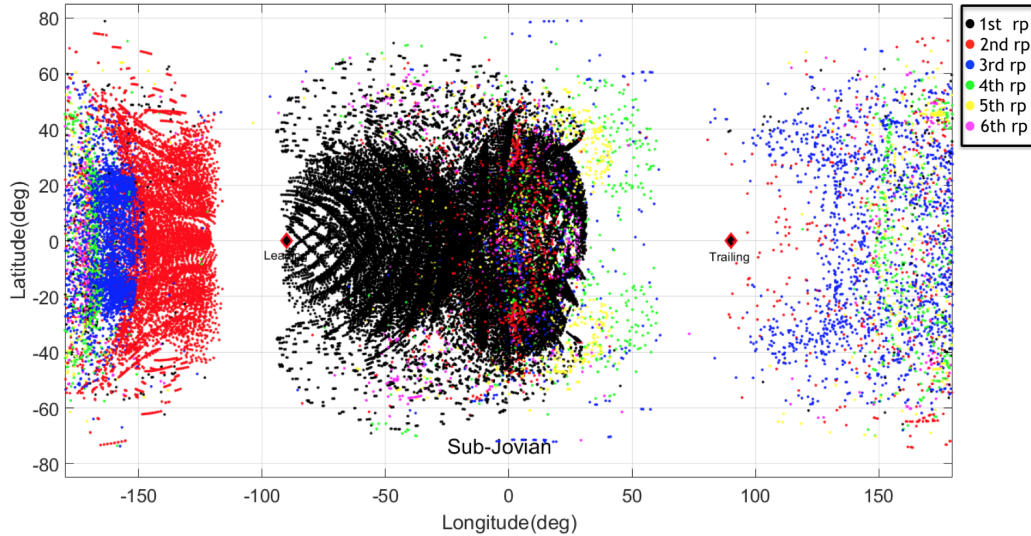


Figure 11. Landing site coverage for the entire database of lissajous orbits, colored by periapsis number.

The results presented in Figure 11 show how the implemented strategy provides landing coverage for a wide range of latitudes, i.e., -80 to 80 degrees, and longitudes, with the exception of the narrow gaps around the leading and trailing regions. In Figure 12, the database of landing solutions is shown again in a latitude/longitude map, but this time colored by Jacobi constant. The energy level of the solutions obtained range between 3.0036 (lower limit of the low-energy regime) and 3.0024. Low latitude regions are reachable from manifolds of lissajous orbits in this spectrum of energies. However, higher latitudes are restricted to landing trajectories with energy in the upper limit of the spectrum. For instance, landing sites at 60 (or -60) degrees of latitude are reachable only by landing trajectories with $J < 3.0025$ *.

Landing Trajectory Examples

Each point on the latitude/longitude maps shown in Figures 11 and 12 represents a landing trajectory solution. The points are periapsis of manifold trajectories emerging from lissajous revs. At a given landing site, the landing trajectory can be characterized by four parameters: latitude, longitude, azimuth (γ), and surface velocity (v_s), where the velocity can be interchanged by the Jacobi

*Recall that the energy level is inversely proportional to the Jacobi constant.

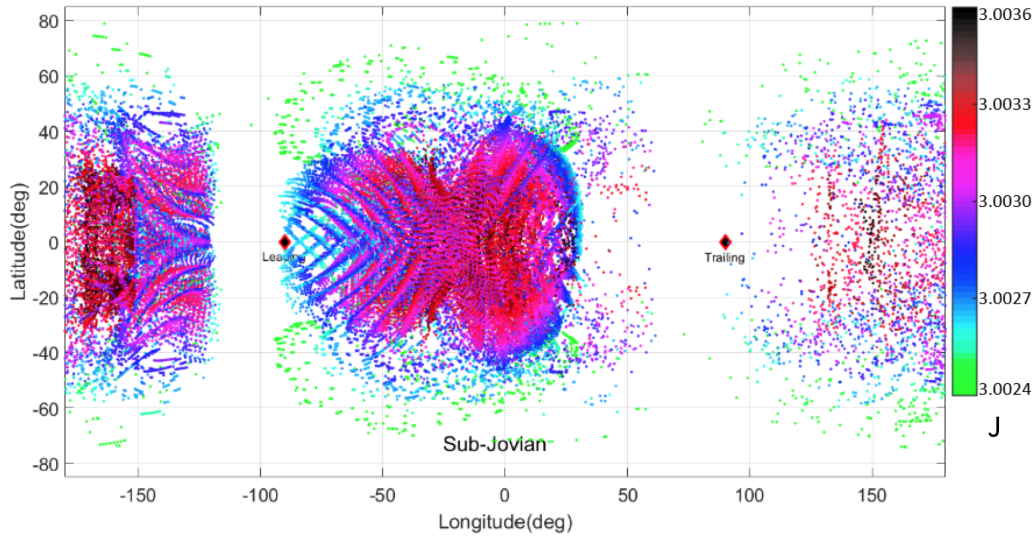


Figure 12. Landing site coverage for the entire database of lissajous orbits, colored by Jacobi constant.

constant. Each landing trajectory is associated to a particular lissajous rev (i.e., A_y , A_z , and ϕ), and a specific value τ , that is, the departure time of the manifold with respect to t_0 of the lissajous rev. Figure 13 shows a landing trajectory that departs from a lissajous rev with parameters $A_y=5500$ km, $A_z=8000$ km, and $\phi=347.4^\circ$, at a time $\tau=0.3$, and connects with a point over the surface of Europa at a longitude= $35^\circ E$, latitude $9^\circ N$, and azimuth $\gamma=164.5^\circ$. The trajectory arrives at the surface with a velocity $vs=1888$ m/s (J) at its third periapsis pass. In Figure 14 a set of representative examples of landing trajectories for different landing sites, with different sets of parameters are presented.

Note from Figure 11 that different landing trajectories solutions can reach the same landing sites. This diversity of solutions is more predominant for low latitudes and regions around the sub-Jovian and anti-Jovian sides, where a high density of points is observed (Figure 11). Different solutions have different arrival geometries (i.e., different azimuths), different energy levels, and different landing times. Having multiple trajectory solutions available for each landing site provides better flexibility for the design.

CONNECTION BETWEEN LANDING TRAJECTORIES AND RESONANT ORBITS VIA BACKWARD INTEGRATION

Once a landing trajectory and its associated lissajous rev is selected, the trajectory that connects the moon tour with the lissajous rev can be designed independently, since the problem has been decoupled. The arrival trajectory (or capture segment) is computed by performing the analysis depicted in Figure 7. This procedure allows to chose an arrival leg that connect with different possible resonances.

Since the capture leg and the landing trajectory are computed independently, it is necessary to ensure that the arrival to the lissajous, i.e., $\tau_{arrival} < \tau_{departure}$ (see Figure 15). To avoid any time conflict, the lissajous rev is recomputed from the departure point, one rev (or several if necessary) backward

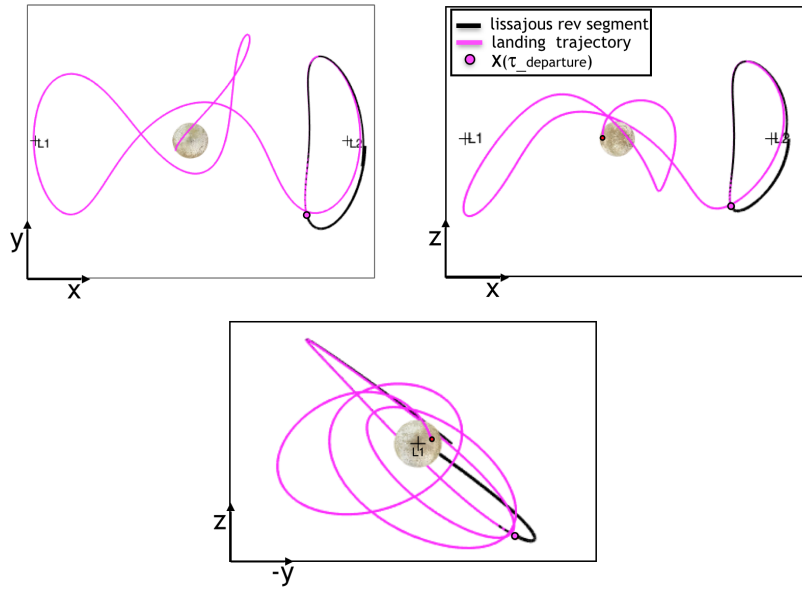


Figure 13. Landing trajectory (magenta) connecting with the site $\{35^\circ E, 9^\circ N\}$, with $\gamma = 164.5^\circ$, and associated $\tau = 0.33^\circ$. Lissajous rev (black) with $A_y=5500$ km, $A_z=8000$ km and $\phi = 347.4^\circ$, $J=3.00283$

on time. Thus, the landing trajectory will always depart at $\tau = 1$ with respect to the recomputed lissajous rev. The new rev is then used to generate the stable manifold (backward in time) that will provide the connection with a resonant orbit. Figure 15 shows a landing solution that connects to a site of longitude= $36^\circ E$, latitude $6^\circ N$. In this example, the capture leg is chosen to connect with a 5:6 resonance. The time spent on the lissajous rev is $\tau_{arrival} - \tau_{departure} = 0.19$, equivalent to 8.8 hours, while the landing trajectory segment has a time of flight of 3.3 days.

From the set of trajectories that arrive to a particular lissajous rev (stable manifolds), there are generally two opportunities to connect with a specific resonance, due to the sinusoidal function between sma and τ (see Figure 7). This feature adds a timing flexibility. Additionally, if a longer staging time is required, the spacecraft can be allowed to stay for multiple lissajous revs. Variations on the magnitude of the perturbation size ϵ , used to compute the manifold trajectories (Eq. 2), can also be used to tune the phase of the arrival and departure time of the trajectories (similar to that described in Lantoine and Russell¹⁴). Any of these strategies can be used to adjust the landing time, and decouple it with the moon tour phase. Figure 16 shows a landing solution that connects to a site of longitude= $44^\circ W$ and latitude $3^\circ N$, including the capture leg, chosen to connect with a 6:7 resonance. In this example, the spacecraft is allowed to stay on the lissajous staging orbit for about two revs. The time spent on the staging orbit is equivalent to 3.2 days, and the landing trajectory segment has a duration of 1.93 days.

CONCLUSIONS

In this paper a strategy to construct low-energy landing trajectories that cover a broad range of landing sites on the surface of Europa is developed. The proposed strategy uses lissajous orbits and their approximate invariant manifolds as building blocks. Lissajous trajectories are used as staging orbits, allowing to decouple the landing and the capture phase of the mission. The approximate unstable manifolds of these orbits provide a rich set of potential landing segments, while their stable

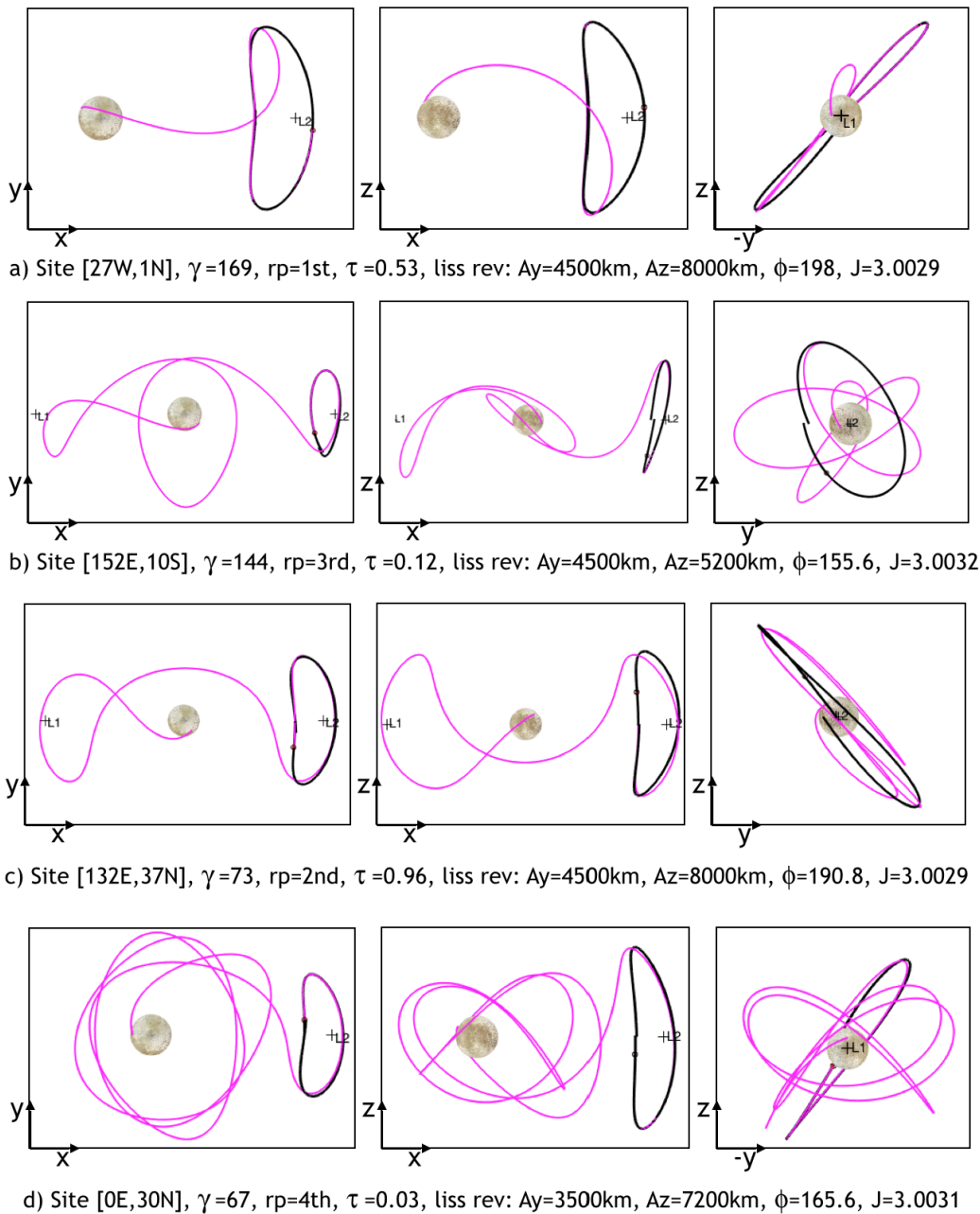


Figure 14. Representative set of landing trajectory solutions.

manifolds (propagated backward in time) allow a connection with resonant orbits, which is usually the last part of a tour approaching Europa. Solving the problem by parts allows to study each phase individually, reducing the complexity of the problem.

Lissajous orbits conform invariant tori. To simplify the computation of their invariant manifolds, individual revs of lissajous orbits are used instead, and each rev is used as an approximate periodic orbit. This discretization allows a systematic way to generate a database of lissajous revs and their approximate invariant manifolds. Millions of approximate manifold segments are generated and

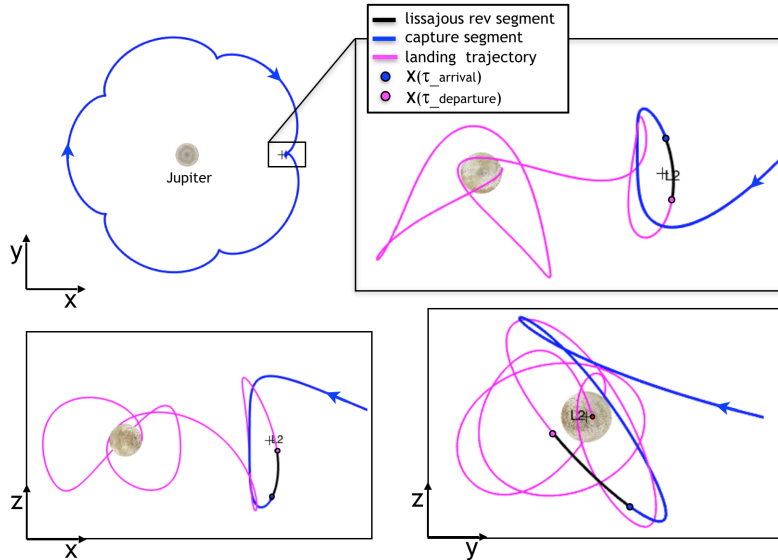


Figure 15. Resonant (5:6) capture and Landing trajectory to site $\{36^\circ E, 6^\circ N\}$, connected through a lissajous rev segment. $J=3.00311$

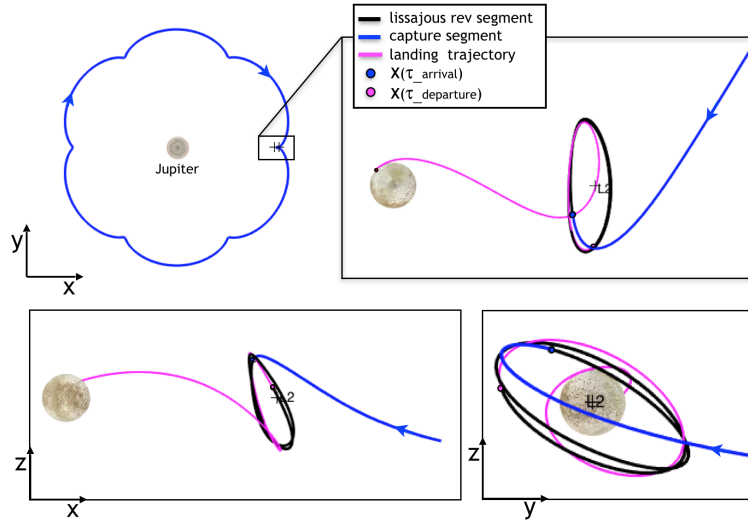


Figure 16. Resonant (6:7) capture and Landing trajectory to site $\{44^\circ W, 3^\circ N\}$, connected through a double lissajous rev segment. $J=3.00338$

searched for potential landing trajectories. The selected solutions provide landing trajectories that reach many points on the surface of Europa, including both high and low latitudes, giving a global range of possible landing locations. Gaps near the trailing and leading edges of Europa, where the natural flow of the lissajous manifolds do not reach, are observed. High latitude sites are reachable only by lissajous revs associated with a high out-of- plane component and a high energy level (low Jacobi constant). In contrast, a high density of solutions are obtained for low latitude sites. A range of resonant orbits is reachable by the approximate stable manifolds of each individual lissajous rev, and this range is only a function of the energy of the rev. Even though the proposed methodology provides a wide coverage of landing sites, lissajous trajectories are highly unstable, and therefore,

station keeping analysis needs to be included in further steps of the design process.

ACKNOWLEDGEMENTS

This study have been partially funded by the NASA Europa Lander mission at the Jet Propulsion Laboratory. Part of this research was carried out at University of Texas, Austin, TX. Part of this research was carried out at the Jet Propulsion Laboratory, California Institute of Technology, under a contract with the National Aeronautics and Space Administration.

REFERENCES

- [1] G. M. Marion, C. H. Fritsen, H. Eicken, and M. C. Payne, "The Search for Life on Europa: Limiting Environmental Factors, Potential Habitats, and Earth Analogues," *Astrobiology*, Vol. 3, No. 4, 2003, pp. 785–811.
- [2] K. P. Hand, R. W. Carlson, and C. F. Chyba, "Energy, Chemical Disequilibrium, and Geological Constraints on Europa," *Astrobiology*, Vol. 7, No. 6, 2007, pp. 1006–1022.
- [3] W. Koon, M. Lo, J. Marsden, and S. Ross, "Constructing a Low Energy Transfer Between Jovian Moons," *Contemporary Mathematics*, Vol. 292, 2001, pp. 129–145.
- [4] S. Campagnola and R. P. Russell, "Endgame Problem Part 2: Multi-Body Technique and the Tisserand-Poincare Graph," *Journal of Guidance, Control, and Dynamics*, Vol. 33, March-April 2010, pp. 476–486, 10.2514/1.44290.
- [5] J. Johannesen and L. D'Amario, "Europa orbit mission trajectory design," *AAS/AIAA Astrodynamics Specialist Conference*, AAS No. 99-360, Girdwood, Alaska, August 15-19, 1999.
- [6] G. J. Whiffen and T. Lam, "The Jupiter Icy Moons Orbiter Reference Trajectory," *AAS/AIAASpace Flight Mechanics Meeting*, No AAS 06-186, Tampa, FL., January 22-26 2006.
- [7] K. Kloster, A. Petropoulos, and J. Longuski, "Europa Orbiter tour design with Io gravity assists," *Acta Astronautica*, Vol. 68, No. 7-8, 2011, pp. 931–946.
- [8] T. McElrath, S. Campagnola, and N. Strange, "Riding the Banzai Pipeline at Jupiter: Balancing Low ΔV and Low Radiation to Reach Europa," *AAS/AIAA Astrodynamics Specialist Conference*, AIAA 2012-4809, Minneapolis, Minnesota, August 2012, pp. 1–13., 2012.
- [9] S. Campagnola, B. Buffintong, and A. Petropoulos, "Jovian tour design for orbiter and lander missions to Europa," *Acta Astronautica*, Vol. 100, February 2014, pp. 68–81.
- [10] S. Ross and D. J. Scheeres, "Multiple Gravity Assists, Capture, and Escape in the Restricted Three-body Problem," *SIAM Journal on Applied Dynamical Systems*, Vol. 6, No. 3, 2007, pp. 576–596, 10.1137/060663374.
- [11] S. Campagnola, P. Skerritt, and R. P. Russell, "Flybys in the Planar, Circular, Restricted, Three-Body Problem.," *Celestial Mechanics and Dynamical Astronomy*, Vol. 113, June 2012, pp. 343–368, 10.1007/s10569-012-9427-x.
- [12] G. Lantoine, R. P. Russell, and S. Campagnola, "Optimization of Low-Energy Resonant Hopping Transfers Between Planetary Moons," *Acta Astronautica*, Vol. 68, April-May 2011, pp. 1361–1378, 10.1016/j.actaastro.2010.09.021.
- [13] W. S. Koon, M. W. Lo, J. E. Marsden, and S. D. Ross, "Heteroclinic Connections Between Periodic Orbits and Resonance Transitions in Celestial Mechanics," *Chaos*, Vol. 10, June 2000, pp. 427–469, 10.1063/1.166509.
- [14] G. Lantoine and R. P. Russell, "Near Ballistic Halo-to-Halo Transfers between Planetary Moons," *The Journal of the Astronautical Sciences*, Vol. 58, No. 3, 2011, pp. 335–363, 10.1007/BF03321174.
- [15] R. L. Anderson, "Approaching Moons from Resonance via Invariant Manifolds," *Journal of Guidance, Control, and Dynamics*, Vol. 38, No. 6, 2015, pp. 1097–1109, 10.2514/1.G000286.
- [16] S. D. Ross, W. S. Koon, M. W. Lo, and J. E. Marsden, "Design of a Multi-Moon Orbiter," *Advances in the Astronautical Sciences*, Vol. 114, 2003, pp. 669–684.
- [17] T. Lam and G. J. Whiffen, "Exploration of Distant Retrograde Orbits Around Europa," *15th AAS/AIAA Space Flight Mechanics Conference*, Copper Mountain, Colorado, Jan. 2005.
- [18] R. P. Russell and T. Lam, "Designing Ephemeris Capture Trajectories at Europa Using Unstable Periodic Orbits," *Journal of Guidance, Control, and Dynamics*, Vol. 30, March-April 2007, pp. 482–491, 10.2514/1.22985.

- [19] D. J. Grebow, A. E. Petropoulos, and P. A. Finlayson, "MULTI-BODY CAPTURE TO LOW-ALTITUDE CIRCULAR ORBITS AT EUROPA," *AAS/AIAASpace Flight Mechanics Meeting, No AAS 11-427*, New Orleans, LA, February 13-17 2011.
- [20] K. Bokelmann and R. P. Russell, "Halo Orbit to Science Orbit Captures at Planetary Moons," *Acta Astronautica*, Vol. 134, May 2017, pp. 141–151.
- [21] D. J. Scheeres, M. D. Guman, and B. F. Villac, "Stability Analysis of Planetary Satellite Orbiters: Application to the Europa Orbiter," *Journal of Guidance, Control, and Dynamics*, Vol. 24, No. 4, 2001, pp. 778–787.
- [22] E. Kolemen, N. J. Kasdin, and P. Gurfil, "Multiple Poincaré Sections Method for Finding the Quasiperiodic Orbits of the Restricted Three Body Problem," *Celestial Mechanics and Dynamical Astronomy*, Vol. 112, No. 1, 2012, pp. 47–74.
- [23] A. Jorba, "Numerical Computation of the Normal Behavior of Invariant Curves of n-Dimensional Maps," *Nonlinearity*, Vol. 14, No. 5, 2001, pp. 943–976.
- [24] A. Jorba and E. Olmedo, "On the Computation of Reducible Invariant Tori in a Parallel Computer," *SIAM Journal on Applied Dynamical Systems*, Vol. 8, No. 4, 2009, pp. 1382–1404.
- [25] F. Schilder, H. M. Osinga, and W. Vogt, "Continuation of Quasi-Periodic Invariant Tori," *SIAM Journal on Applied Dynamical Systems*, Vol. 4, No. 3, 2005, pp. 459–488.
- [26] Z. P. Olikara and D. J. Scheeres, "Numerical method for computing quasi-periodic orbits and their stability in the restricted three-body problem," *Advances in the Astronautical Sciences*, Vol. 145, No. 911-930, 2012.
- [27] J. M. Mondelo, E. Barrabés, G. Gómez, and M. Ollé, "Fast Numerical Computation of Lissajous and Quasi-Halo Libration Point Trajectories and Their Invariant Manifolds," *In 63rd International Astronautical Congress, International Astronautical Federation*, 2012.
- [28] K. Howell and H. Pernicka, "Numerical Determination of Lissajous Trajectories in the Restricted Three-Body Problem," *Celestial Mech.*, Vol. 41, 1988, pp. 107–124.
- [29] D. L. Richardson and N. D. Cary, "A Uniformly Valid Solution for Motion About the Interior Libration Point of the Perturbed Elliptic-Restricted Problem," *AAS/AIAA Astrodynamics Specialist Conference, Nassau, Bahamas, July 28-30, 1975*.
- [30] Z. P. Olikara and K. C. Howell, "Computation of Quasi-Periodic Invariant Tori in the Restricted Three-Body Problem," *Advances in the Astronautical Sciences*, Vol. 136, No. 313-327, 2010.
- [31] T. Lam, J. J. Arrieta-Camacho, and B. Buffintong, "The Europa Mission: Multiple Europa Flyby Trajectory Design Trades and Challenges," *AAS/AIAA Astrodynamics Specialist Conference, AAS No. 15-657, Vail, CO, August 2015*, 2015.
- [32] L. Try, B. B. Buffintong, and S. Campagnola, *A Robust Mission Tour for NASA's Planned Europa Clipper Mission*. American Institute of Aeronautics and Astronautics, 2018/06/13 2018, doi:10.2514/6.2018-0202.
- [33] R. L. Restrepo and R. P. Russell, "Patched Periodic Orbits: A Systematic Strategy for Low-Energy Transfer Design," *AAS/AIAA Astrodynamics Specialist Conf., AAS 17-695*, Stevenson, WA, Aug. 2017.
- [34] R. L. Restrepo and R. P. Russell, "A Database of Planar Axisymmetric Periodic Orbits for the Solar System," *Celestial Mechanics and Dynamical Astronomy*, Vol. 130, July 2018, p. 49, 10.1007/s10569-018-9844-6.
- [35] G. Gómez, W. S. Koon, M. W. Lo, J. E. Marsden, J. J. Masdemont, and S. D. Ross, "Connecting orbits and invariant manifolds in the spatial restricted three-body problem," *Nonlinearity*, Vol. 17, September 2004, pp. 1571–1606.
- [36] K. C. Howell, "Three-Dimensional, Periodic, 'Halo' Orbits," *Celest. Mech.*, Vol. 32, 1984, pp. 53–71.
- [37] G. Gómez, J. J. Masdemont, and C. Simó, "Quasihalo Orbits Associated with Libration Points," *Journal of Astronautical Science*, Vol. 46, No. 2, 1998, pp. 135–176.
- [38] R. Farquhar and A. Kamel, "Quasi-Periodic Orbits About the Translunar Libration Point," *Celestial Mechanics and Dynamical Astronomy*, Vol. 7, No. 4, 1973, pp. 458–473.
- [39] A. Jorba and J. J. Masdemont, "Dynamics in the Center Manifold of the Restricted Three-Body Problem," *Physica*, Vol. 132, No. 1-2, 1999, pp. 189–213.
- [40] B. T. Barden and K. C. Howell, "Formation Flying in the Vicinity of Libration Point Orbits," *Advances in the Astronautical Sciences*, Vol. 99(z), 1998, pp. 969–988.
- [41] G. Gómez and J. M. Mondelo, "The Dynamics Around the Collinear Equilibrium Points of the RTBP," *Physica*, Vol. 157, No. 4, 2001, pp. 283–321.